

Advanced Radiometric & Interferometric Millimeter-Wave Scene Simulations

B. I. Hauss, P. J. Moffa, W. G. Steele, H. Agravante, R. Davidheiser, T. Samec
and S. K. Young
TRW Space and Electronics Group

1.0 Introduction:

Smart munitions and weapons utilize various imaging sensors (including passive IR, active and passive millimeter-wave, and visible wavebands) to detect/identify targets at short standoff ranges and in varied terrain backgrounds. In order to design and evaluate these sensors under a variety of conditions, a high-fidelity scene simulation capability is necessary. Such a capability for passive millimeter-wave scene simulation exists at TRW. TRW's Advanced Radiometric Millimeter-Wave Scene Simulation (ARMSS) code is a rigorous, benchmarked, end-to-end passive millimeter-wave scene simulation code for interpreting millimeter-wave data, establishing scene signatures and evaluating sensor performance.

In passive millimeter-wave imaging, resolution is limited due to wavelength and aperture size. Where high resolution is required, the utility of passive millimeter-wave imaging is confined to short ranges. Recent developments in interferometry have made possible high resolution applications on military platforms. Interferometry or synthetic aperture radiometry allows the creation of a high resolution image with a sparsely filled aperture. Borrowing from research work in radio astronomy, we have developed and tested at TRW scene reconstruction algorithms that allow the recovery of the scene from a relatively small number of spatial frequency components.

In this paper, the TRW modeling capability is described and numerical results are presented.

2.0 The ARMSS Code:

The radiometric signature of a man-made, highly reflecting target depends sensitively on the target geometry and the background (sky and/or terrain) brightness temperatures which happen to lie along the specular reflection path. It is thus critical to describe these elements accurately. To model the interaction between the target, the sky/terrain background and the radiometer, TRW has developed ARMSS, a rigorous, benchmarked, end-to-end passive millimeter-wave scene simulation code. Many of the physics models employed are "first principles"-models, requiring only measurable physical conditions to accurately predict millimeter-wave scene signatures. In addition, our models offer a true

3-D scene simulation capability, allowing the complex interactions between the various elements of the scene to be correctly described. This is required at millimeter-wave frequencies both because the downwelling atmospheric radiation varies dramatically with zenith angle and because the emissivity/ reflectivity of most terrain materials has a significant dependence on incidence angle. This is especially true near grazing incidence, where scattering and emission are further complicated on rough surfaces by multiple scattering and shadowing effects.

The four major components of the ARMSS code are shown in Figure 2.1. The first and primary component of this end-to-end code is a rigorous description of the passive mm wave phenomenology. This encompasses state-of-the-art physics models describing: emission from the scene constituents, scattering of the downwelling sky radiation by the scene, propagation/attenuation of the electromagnetic energy from the scene to the sensor, and upwelling atmospheric radiation between the scene and the sensor. More specifically, the phenomenology model includes sub-models for atmospheric propagation effects and meteorology, surface/terrain physics describing the mix of emission and scattering from scene constituents, ray-tracing algorithms for efficient but accurate solution of the radiative transfer equation, and the use of combinatorial geometry for constructing complex three-dimensional scenes, Figure 2.2. Each aspect of the phenomenology model has been individually benchmarked against both measured data and other models in the literature. In addition, the phenomenology model as a whole has been benchmarked against the field-imaging data which we have collected.

The second component of the end-to-end simulation code, the sensor model, takes output from the phenomenology model (i.e., the very high resolution, radiometric image in front of the sensor) and constructs the actual image as seen by the sensor, based on diffraction optics and including such effects as lens aberrations, finite detector size, and noise. This allows us to assess sensor performance and perform design tradeoffs. Again, all aspects of the sensor model have been benchmarked.

Next, to evaluate the ability of real-time image enhancement and restoration techniques to improve image quality, thereby allowing tradeoffs to be made with the sensor design requirements, an image processing capability has been included in the end-to-end code. This takes as input raw data from the sensor and applies noise filtering, upsampling, temperature bandpass filtering, global and hybrid histogram equalization, and edge-operator sharpening techniques to enhance the resulting image and thereby allow some relaxation of the sensor design requirements.

The display model, the final component of the end-to-end code, captures the enhanced images, frame-by-frame, on video tape for replay at the frame-rate for which the images were produced. This allows us to perform those sensor design tradeoffs which involve frame-rate, where higher frame rates normally result in a poorer signal-to-noise ratio.

Because of their importance to the accurate generation of passive millimeter-wave scenes, a more detailed description of the models describing atmospheric propagation and the

calculation of the sky radiometric temperature profile, terrain emissivity/ scattering, and the construction of the background-target scene geometry will be given in sub-sections 2.1-2.3 below.

2.1 Atmospheric Propagation and Sky Radiometric Temperature Calculations

The sky radiometric temperature profile (a function of zenith angle) is calculated within the ARMSS code based on computations of the downwelling atmospheric radiation. These calculations begin with a determination of the specific attenuation rates in the atmosphere. To this end, the propagation effects model developed by the Institute for Telecommunication Sciences (Reference 1) has been implemented in the code. The model calculates the specific attenuation rates as a function of measurable meteorological parameters (pressure, thermometric temperature, relative humidity, hydrosol concentration and rain rate) and has a range of validity from 0 to 1000 GHz. The model includes pressure broadened resonance lines for water and oxygen, continuum absorption due to non-resonant oxygen, pressure induced nitrogen absorption, Rayleigh absorption for haze, fog and clouds, and a parameterized power-law rain attenuation model to simulate Mie scattering and absorption by a distribution of droplet sizes corresponding to a measured rain rate. The model accurately compares with published and measured data for clear-air, fog, and rain attenuation, Figure 2.1.1.

To provide meteorological properties as a function of altitude for diverse geographic and seasonal changes in atmospheric conditions, the ARMSS code makes use of any of ten synthetic atmospheric databases compiled by the Air Force Geophysics Laboratory. This allows the code to accommodate a diverse range of climatological and weather conditions, ranging from subtropical to arctic and in various seasons. In addition, plane-stratified (i.e., layer) models for clouds, fog, haze and rain are included in the code to allow study of their effects, both individually and collectively.

The sky radiometric temperature profile is calculated by a detailed evaluation of the radiative transfer equation for the downwelling atmospheric radiation, taken from 30 km above sea-level. The highly efficient ray tracing solution permits some 60,000 rays to be processed in only 7 minutes on a Silicon Graphics Personal Iris. Benchmarks with the literature and field measurements, using the 1976 U.S. Standard Atmospheric data base to provide meteorological properties, have been performed, Figure 2.1.2.

The models described above are also used in computing both the upwelling atmospheric radiation and the attenuation of the scattered and/or emitted radiation between elements of the scene and the sensor. A benchmark of these calculations, including the contributions due to terrain emission and scattering is discussed in the following sections.

2.2 Terrain Emissivity/Scattering Calculation

Terrain emissivities/reflectivities are calculated within the ARMSS code based on the dielectric properties of the terrain layer(s) and their surface/subsurface geometry. For a

single smooth (i.e., specular) layer, emissivity/reflectivity is determined from a straightforward calculation of the Fresnel reflection coefficient, which depends only on the angle of incidence and the complex dielectric constant of the terrain material.

The emissivity/reflectivity for multiple smooth dielectric layers is obtained from a calculation of either the coherent or incoherent multiple layer effective reflectivity, depending on whether phase coherence is maintained within the layers (i.e., whether volume scattering within the layers is significant). The coherent reflectivity is calculated by rigorously solving for the electromagnetic fields in each dielectric layer and then employing a matrix technique to combine their individual effects, always requiring phase accountability, to give the effective field reflection coefficient at the terrain surface. Squaring the magnitude of this quantity then gives the coherent power reflection coefficient. For the calculation of the incoherent reflectivity, reflections from each layer are treated as an incoherent process, avoiding phase effects by basing all calculations on the power (i.e., Fresnel) reflection coefficient for each layer. This calculation is carried to infinite order in the number of reflections at the layer boundaries. For the three-layer problem, this results in a closed-form expression for the effective surface power reflection coefficient. Finally, assuming that the thermometric temperature is the same for all the terrain layers, the emissivity for either the coherent or incoherent process is the difference between unity and the calculated reflectivity.

For the rough surface emissivity, we employ either the semi-empirical model of Choudhury and Wang (Reference 2), with roughness parameters chosen to give the best fit to measured data, or Wagner-Lynch (Reference 3) scattering theory for an anisotropic, random rough surface characterized by Gaussian statistics. This latter approach is based on a geometrical-optics theory of emission and scattering. A complete ray treatment is provided in the sense that single-scatter and bistatic shadowing effects are included in a consistent manner for a general two-dimensional rough surface. To conserve energy to a relatively high degree of approximation for all observation angles, a double-scatter approximation is usually required. However, the single-scatter approximation employed in the code provides predicted radiometric temperatures within a few Kelvin of the true temperatures over most observation angles, Figure 2.2.1.

A data-base of models describing the dielectric properties of naturally occurring and man-made terrain materials (water-fresh and sea, ice-fresh and sea, snow, various types of soils, asphalt, concrete, etc.) has been developed for use in calculating terrain emissivities. For the majority of materials, these models are given as a function of frequency, physical temperature, density, and water content. The bulk dielectric mixing models for some materials are setup using a specified material makeup (e.g., the various soil categories use specified bulk densities and percentages of sand, silt, and clay) as a user convenience. This convention is easily modified to allow any appropriate combination of parameters as determined by measurement of the local properties. These models have been successfully compared to published data, Figure 2.2.2.

2.3 Three-Dimensional Background-Target Scene Generation

Atmospheric propagation and terrain surface interaction models are joined through the use of a true 3-D ray tracing solution of the radiative transfer equation. This model determines ray paths through the atmosphere and ray intercepts with scene objects. The model first employs a backward tracing of the ray paths, from the sensor, through multiple reflections off scene objects and upward through the atmosphere. A forward integration of the radiative transfer equation along the calculated ray path then gives the radiometric temperature at a single point in the infinite resolution image at the pupil plane in front of the sensor. Figure 2.3.1 shows four snapshot simulations of an aircraft landing on a concrete runway surrounded by dirt. The weather conditions are heavy fog with wet ground surfaces. A plane is parked on an adjacent taxi-way, with its reflected image on the nearby terrain surface. The important point to note is that this is a complex scene viewed at near grazing incidence on both specular and rough terrain surfaces which is realistically modeled.

The fidelity of the combined models for atmospheric propagation, terrain emission and scattering, and the numerical solution of the radiative transfer equation has been extensively benchmarked by comparisons with field measurements, Figures 2.3.2. These results indicate that the models are not only qualitatively correct, but also quantitatively accurate.

To achieve an efficient and highly accurate 3-D scene description, the ARMSS code employs combinatorial geometry (also known as constructive solid geometry) to model both elements of the terrain and high-value targets in the scene. The mathematical description of each object in the scene is achieved through the orderly combination of any of eight basic solid geometric primitives; rectangular parallelepiped, box, sphere, right circular cylinder, right elliptical cylinder, truncated right angle cone, ellipsoid of revolution, and right angle wedge. A scene object's location and shape is described by selecting the appropriate geometric primitives and specifying their location, dimensions, and how to combine them (given in terms of the unions, intersections, and exclusions, of their individual volumes), Figure 2.3.3. As can be seen from the constructed models for the BMP-1 troop transport, the T-72 tank and the SS-24 missile and mobile launcher (Figure 2.3.4), this approach affords an accurate representation of scene objects, with true surface curvatures which would be extremely difficult to achieve from a faceted geometry model. The requirement to accurately predict the millimeter-wave scene obviously dictates the need for this accurate treatment of the scene geometry.

In addition to determining the path length from the ray's current position to its next intersection with a scene surface, the geometry package also identifies the code surface element intersected, the angle of the incident ray to the surface, and the normal to the surface at the point of intersection. This information is necessary in modelling the contributions to the radiometric temperature from the terrain surface. In particular, the identification of the code surface element intersected provides the terrain/surface physics models with the particular surface and subsurface properties (specified as input for each surface element) at the point of intersection. These properties include the number of

dielectric layers for the surface element, specification of either coherent or incoherent scattering/emission (for code surface elements having multiple dielectric layers), layer material type, layer water content, layer density, surface thermometric temperature, and parameters specifying the surface rms roughness slope.

2.4 Real-Time Passive Millimeter Wave Scene Simulation:

As part of a joint program with NASA LaRC, TRW has been developing a real-time, passive millimeter wave scene simulation capability. The general approach taken to achieve real-time operation has been to identify the necessary passive millimeter wave phenomenology models from TRW's ARMSS code and implement these in an approximate fashion into NASA's visible flight simulator. The primary requirement on this process was that it maintains reasonable scene fidelity without sacrificing real-time performance. The approximations made are summarized in Table 2.4.1 and described briefly below.

First, the Constructive Solid Geometry (CSG) description of the terrain scene was replaced with a polygonal tessellation. This allowed us to replace the high ray sampling of the CSG scene with a much reduced (by a factor of 1000 or more) ray tracing only to the verticies of the polygonal scene elements. Polygon shading between the verticies is performed by simple shading models implemented in the Silicon Graphics firmware. This introduces a small interpolation error in the scene radiances between polygon verticies; however, the magnitude of this interpolation error is easily controlled by reducing the size of the scene polygons. A second problem introduced by the polygonal scene element approach is the difficulty in simulating multiple reflections and shadowing effects, although a method has been devised for implementing these as well.

The second group of approximations which were required to achieve real-time passive millimeter wave scenes were the use of lookup tables. The real-time code employs lookup tables for the sky temperature profile, the emissivity/reflectivity of specular-surface scene elements versus

incidence angle, and the apparent temperature of rough-surface terrain elements as a function of the angle of observation and assuming a horizontal mean ground-plane. These tables are computed at the beginning of the simulation based on the input atmospheric and terrain conditions. This use of lookup tables eliminates the need for repetitive calculations of the downwelling atmospheric radiation and the emitted and scattered radiation from the scene elements for each ray. There is a small price incurred in terms of interpolation error, but as will be illustrated in the following talk from NASA LaRC, these errors are negligible.

A significant improvement in performance, which allowed real-time operation, resulted from the approximation for the upwelling atmospheric radiation from a scene element to the sensor. Since the sensor is continuously moving and viewing different elements of the terrain, this calculation could not be handled using a lookup table. The approximation employed makes use of the fact that the temperature lapse rate in the troposphere is small, only 6.5K/km. This means that over a plane stratified layer of perhaps a few tenths of kilometers in height, the thermometric temperature is essentially constant. Considering that most of the landing simulations will involve sensors within 0.2km of the ground, the integral of the path radiance from the scene element to the sensor,

$$\int_0^L \alpha(s') T(s') \exp\left[-\int_{s'}^L \alpha(s'') ds''\right],$$

can be reduced to a simple algebraic form

$$T_m \left\{ 1 - \exp[-\tau(0, L)] \right\},$$

where T_m is the effective or mean thermometric temperature along the path and

$$\tau(0, L) \equiv \int_0^L \alpha(s'') ds'' = \sec\theta \tau(0, Z)$$

is the cumulative optical thickness. A lookup table of $\tau(0, z)$ is

computed at the beginning of the simulation, and used to further speedup the calculation. As can be seen from Figure 2.4.1, the difference between a brute-force numerical integration of the path radiance and the above constant temperature approximation is negligible; however, the approximate solution is easily two-orders of magnitude faster.

The final approximation employed in the real-time model is the restriction to a single specular reflection from an element of the scene. The model assumes that any reflection off a scene-element which results in the ray going back towards the terrain will be reflected from the terrain as if from a perfectly conducting horizontal ground plane. This approximation was implemented as a temporary measure until there was sufficient resources to implement a multiple reflection model. A method for implementing multiple reflections and shadowing in real-time using the polygonal model described earlier has been devised, but not yet implemented. The current approach does not correctly treat the interaction between elements of the 3-D scene.

We have benchmarked the real-time passive millimeter wave scene simulation against TRW's ARMSS code, and have found it to be accurate to within a few Kelvin throughout the entire scene. The details of this comparison and a live demonstration of the real-time passive millimeter wave flight simulator will be presented in the following talk by NASA LaRC. The principal planned upgrade to the real-time simulator is the implementation of models for multiple reflection and shadowing, allowing the correct treatment of the interaction of the 3D scene elements.

3.0 Interferometric Modeling:

Interferometry is a technique for trying to achieve the resolution of a large aperture by only sparsely covering the equivalent area with much smaller apertures. The Van Cittert-Zernike Theorem (see for example Reference 4) relates the correlations (called visibilities, V) as measured by each antenna pair of the interferometer with the scene intensity (brightness, I). The visibilities are functions of the two spatial frequencies u and v . These are the x and y components respectively of the antenna spacing (baseline) divided by the wavelength. The Theorem states that V and I are a Fourier pair and thus a simple inversion can be utilized to recover the scene intensity. (Figure 3.1) The sparse array of antennas produces, however, only a fraction of the Fourier coefficients. The modeling techniques described in this section addresses the issue of image reconstruction based on an incomplete Fourier transform. To increase the number of Fourier coefficients measured, or the coverage, one can increase either the number of antennas or the bandwidth. In the latter case, the received bandwidth must be subdivided or channelized to provide discrete Fourier coefficients. The design of an interferometric system relies on striking a balance between hardware and processing.

Besides the problem of trying to determine the scene content by only measuring a fraction of the Fourier coefficients, there is a calibration concern. Errors in each antenna measurement can be attributed to uncertainties in its location relative to the other antennas, atmospheric effects on the signal propagation and errors introduced by hardware imperfections. These errors must be removed through processing.

The Astronomical Image Processing System (AIPS) was acquired from the National Radio Astronomy Laboratory. It contains state-of-the-art algorithms developed by the radio astronomy community for image formation, image processing and self-calibration. (See Reference 5.)

There is a penalty paid for trying to recreate the resolution of a large aperture by only sparsely filling the area with antennas. Large, deterministic but confusing, sidelobes appear in the interferometric image. The radio astronomers have descriptively termed this unprocessed image a "dirty" image. The large sidelobes arise since many of the Fourier coefficients necessary to fully determine the image have not been measured. In the inverse Fourier transform performed to create the image, these unmeasured terms are set to zero. The dirty beam is defined to be the dirty image of a point source at the image center. It is equivalent to the point spread function in optics. It is determined by setting all of the measured correlations to one and then Fourier transforming. It is the response of the interferometer to a point source and is fully deterministic.

The dirty image can be thought of as the convolution of the dirty beam with all the sources in the scene. Clearly, the large sidelobes associated with each of the stronger sources will tend to cover the image and mask the weaker sources. The deconvolution of this dirty beam from the dirty image will lead to a "cleaner" representation of the sources in the scene. This is the goal of the nonlinear deconvolution techniques developed by the radio astronomers. (See, for example, Reference 5.) The two principal ones are CLEAN and MEM (maximum entropy method).

3.1 CLEAN and MEM

CLEAN is a straightforward iterative method for removing the sidelobes from the dirty image and uncovering the true sources. In its simplest form, the pixel with the largest amplitude is located; a dirty beam scaled to a fraction of the peak amplitude (that fraction is termed the gain) and located at the peak is subtracted from the dirty image; a tally of the location and strength of the peak is kept; and the process is repeated until the remaining image (called the residual image) is either flat enough or small enough. At that point, all of the point values stored from the found peaks are combined, convolved with an appropriate "clean" beam, and added to the residual image; The result is the "clean" image. As the stronger sources are located and their associated dirty beams are subtracted, the weaker sources emerge from the sea of sidelobes and image fidelity is dramatically improved.

A more sophisticated version of CLEAN, the Clark algorithm, has been implemented in AIPS. The CLEANING iteration has been split into major and minor cycles, in order to speed up execution. Usually, thousands of iterations are necessary.

The second approach for image cleaning is MEM. It is mathematically more complicated than CLEAN. Unlike CLEAN, which has an underlying assumption that the scene is made up of discrete isolated sources, MEM is a much more general nonlinear deconvolution technique. The premise on which it is based states that there are an infinite number of choices for the values of the unmeasured Fourier coefficients and that setting them to zero, as is done in the dirty image formation, is not the optimum choice. MEM is a prescription for choosing the unknown Fourier coefficients.

With the MEM algorithm, an entropy-like function of the image pixel intensities is constructed. This can be related to the information content of the scene. MEM then chooses the values of the unmeasured Fourier terms by maximizing the "entropy", with the constraint that the measured Fourier coefficients match the Fourier transform of the MEMed image to within the noise. This multi-dimensional, constrained maximization has been implemented in AIPS in an iterative scheme that converges rapidly, usually in ten's of iterations.

The radio astronomers have taken advantage of the fact that the main errors arising in interferometric data collection are associated with each antenna. Since correlations are formed pair-wise, there are many more correlations than errors. An iterative technique,

known as self-calibration. has been developed to remove these errors from the data. This algorithm is included in the AIPS package.

3.2 Modeling Results

In Figure 3.2.1, we show an airport scene generated by the phenomenology module of the ARMSS code. For each specific interferometric configuration, a "mask" depicting the corresponding u-v plane coverage is produced. (See Figure 3.2.2) Using this mask, the appropriate Fourier components that the interferometer will measure are filtered out and stored in a file suitable for input into an image processing code such as AIPS. This scene generation procedure is summarized in Figure 3.2.3. The unprocessed and the processed images (using the CLEAN and the MEM algorithms respectively) of the scene are shown in Figure 3.2.4. Finally, to illustrate self-calibration, random phase noise is injected into the received signals in order to corrupt the interferometric image. The self-calibration algorithms allow for the recovery of the original image as shown in Figure 3.2.5..

4.0 Conclusion:

An end-to-end passive millimeter wave system modeling capability has been developed at TRW and state-of-the-art interferometric image processing codes have been acquired. These codes have been applied extensively to the design of radiometric and interferometric imaging systems for divers commercial and military applications (Reference 6).

References:

1. H. Liebe, "An updated model for millimeter wave propagation in moist air," *Radio Sci.* 20 (1985) 1069
2. F.T. Ulaby, R.K. Moore and A.K. Fung, *Microwave Remote Sensing, Volume 3*, Addison-Wesley Publishing Co., Reading, MA, 1981
3. P.J. Lynch and R.J. Wagner, "Rough-surface scattering: shadowing, multiple scatter, and energy conservation," *Journ.Math.Phys.* 11 (1970) 3032
4. A.R. Thompson, J.R. Moran, and G.W. Swenson, Jr., *Interferometry and Synthesis in Radio Astronomy*, John Wiley and Sons, Inc., New York, NY 1986
5. R.A. Perley, F.R. Schwab, and A.N. Bridle, editors, *Synthesis Imaging*, distributed by the National Radio Astronomy Observatory, 1986
6. S.K. Young, R.A. Davidheiser, B. Hauss, P. Lee, M. Mussetto, M.M. Shoucri, and L. Yujiri, "Passive millimeter-wave imaging", *TRW Quest Mag.*, vol.13, no.2, pp 3-20, Winter 1990/1991

APPROXIMATIONS TO PHENOMENOLOGY FOR REAL-TIME OPERATION

<p>Polygonal tessellation of scene elements, with tracing only to polygon vertices</p>	<p>Much fewer rays to trace (by factor of 1000 or more) permits near-real-time operation</p>	<p>Less accurate description of scene geometry Difficult to simulate reflection Introduces interpolation error in computed temperatures between polygon vertices</p>
<p>Lookup table for sky temperature vs. zenith angle, computed at start of simulation</p>	<p>Saves repetitive integration of rays from top of troposphere for downwelling atmospheric radiation</p>	<p>Negligible interpolation error in sky temperature at arbitrary zenith angle Limited to azimuthally symmetric sky conditions (i.e., no patchy clouds)</p>
<p>Lookup table for emissivity of specular surfaces as a function of incidence angle, computed at start of simulation</p>	<p>Saves repetitive calculation of dielectric properties and single or multiple layer emissivities for terrain surface elements</p>	<p>Negligible interpolation error in computed terrain emissivity at arbitrary incidence angle</p>

Table 2.4.1

APPROXIMATIONS TO PHENOMENOLOGY FOR REAL-TIME OPERATION

<p>Lookup table for rough surface apparent temperature as a function of observation angle (with normal to mean ground plane pointed towards zenith), computed at start of simulation</p>	<p>Saves repetitive calculation of multidimensional integrals for emitted and scattered radiation from anisotropic random rough surfaces</p>	<p>Restricted to ground planes which are close to horizontal Doesn't allow for shadowing by other scene elements Negligible interpolation error in computed apparent temperature at arbitrary angle</p>
<p>Approximate method for treating upwelling atmospheric radiation</p>	<p>Much shorter computation time for evaluation of upwelling atmospheric radiation (by a factor of at least 100) permits real-time operation</p>	<p>Negligible integration error introduced when sensor platform height is within a few kilometers of ground</p>
<p>Single specular reflection model, which assumes second reflection off terrain is from a perfectly conducting, horizontal ground plane</p>	<p>Some computational savings in not having to follow multiply reflected rays</p>	<p>Will not correctly treat the interaction between elements of 3-D terrain and obstacles</p>

Table 2.4.1 (Cont.)

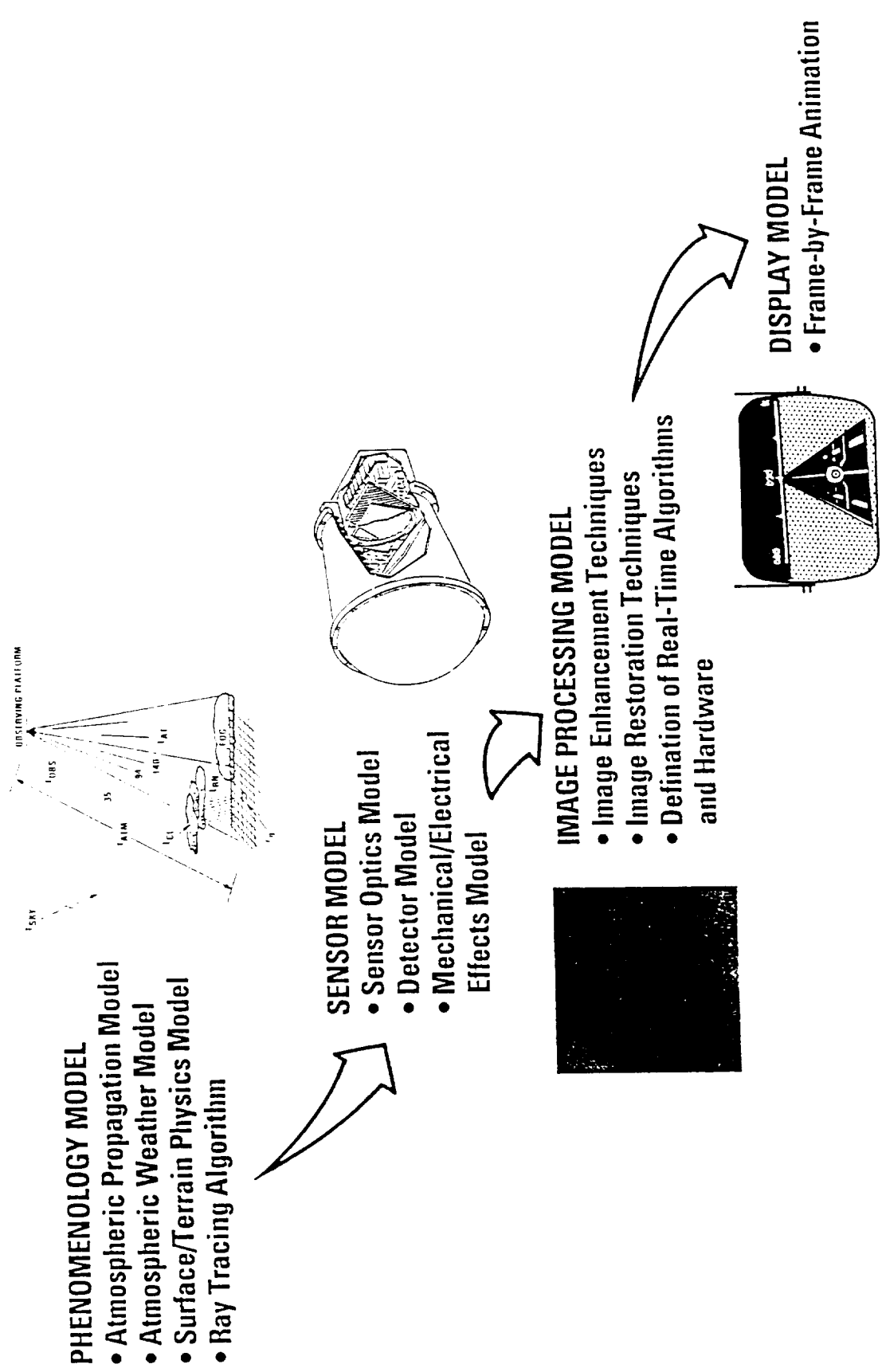


Figure 2.1 Principal Components of TRW's End-to-End Advanced Radiometric Millimeter Wave Scene Simulation Code (ARMSS)

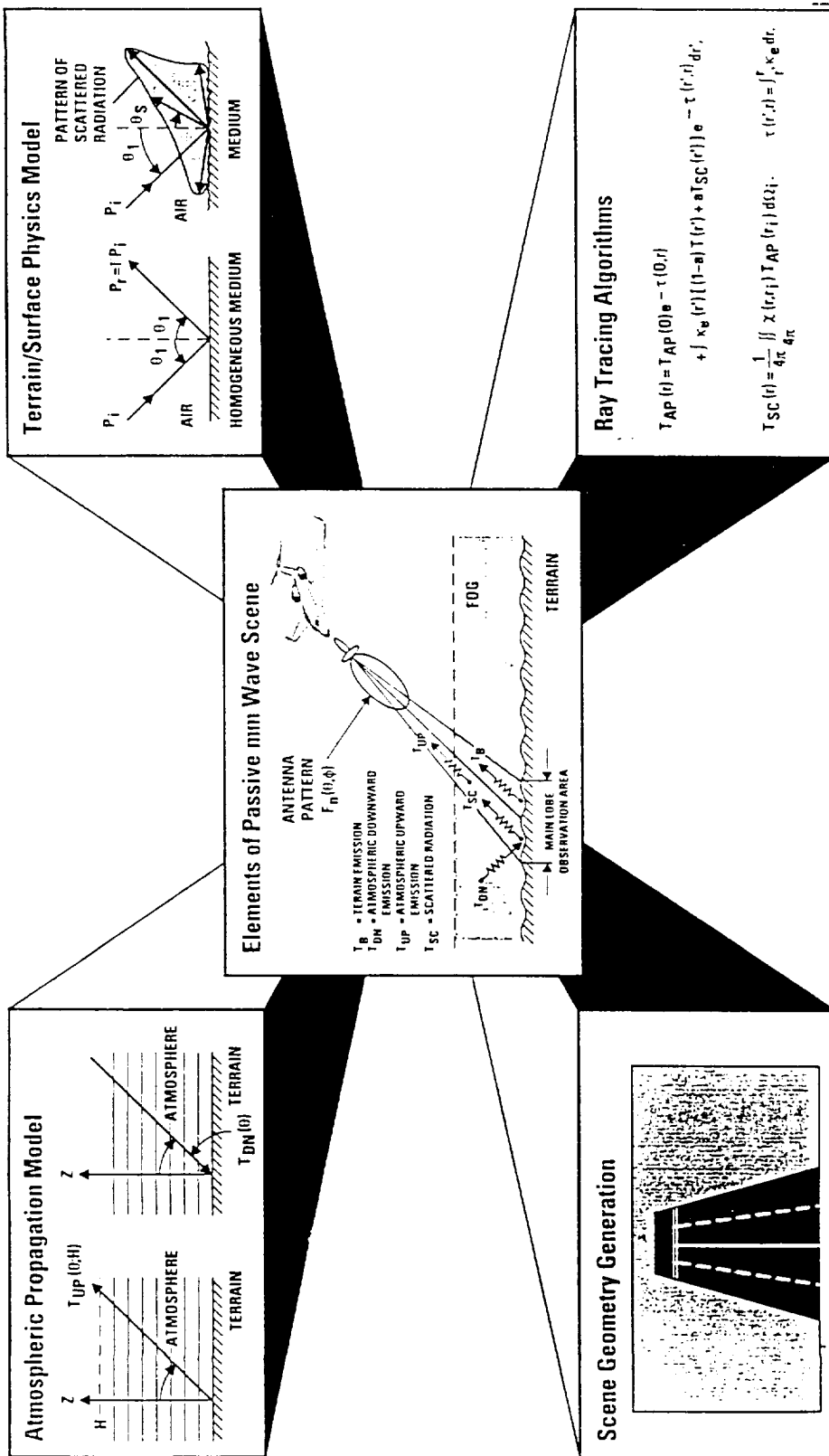
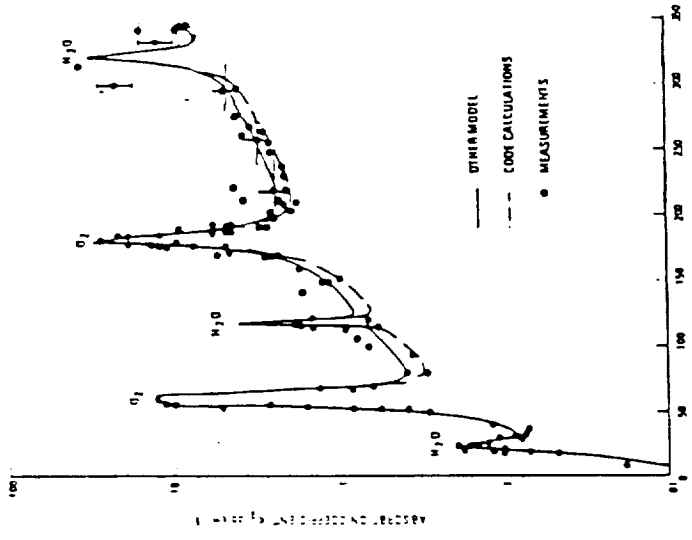
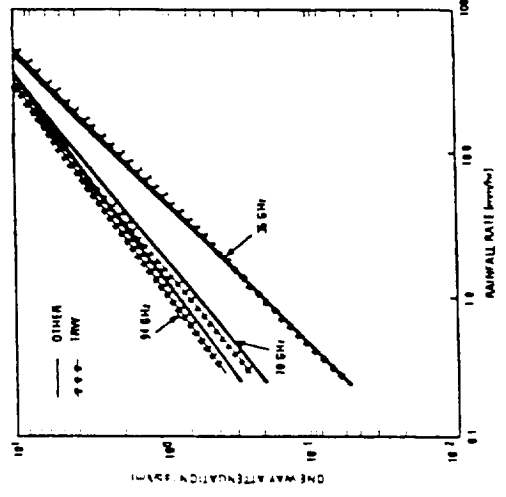


Figure 2.2 Basic Elements of the Passive Millimeter Wave Phenomenology Models in ARMSS

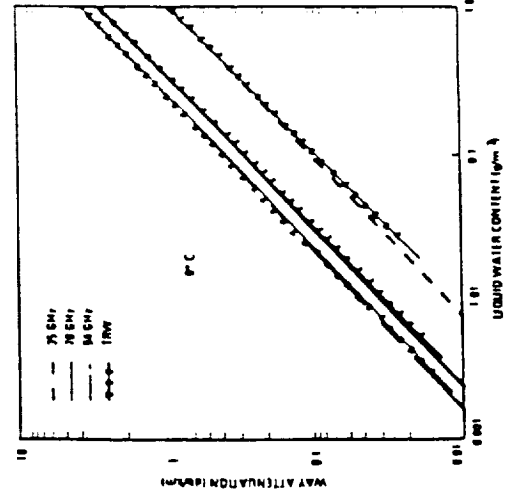
THE TRW MODEL PREDICTS MOIST, CLEAR-AIR ATTENUATION



THE TRW MODEL PREDICTS RAIN ATTENUATION



THE TRW MODEL PREDICTS FOG ATTENUATION



- MOST RECENT VERSION OF POINT ATTENUATION RATE MODEL FROM ITS (H. UEBE)
- CALCULATES RADIO PATH PARAMETERS (ATTENUATION AND PROPAGATION PATH DELAY EFFECTS) FROM METEOROLOGICAL DATA (P - T - RH - W - RH)
- MODEL'S RANGE OF VALIDITY IS 0 - 10000 GHz
- MODEL INCLUDES:
 - PRESSURE BROADENED RESONANCE LINES FOR H₂O (22-997 GHz) AND O₂ (49-834 GHz)
 - CONTINUUM ABSORPTION DUE TO H₂O LINES ABOVE 1 THz AND EMPIRICAL CORRECTIONS REQUIRED BY V-W LINE SHIFTS AWAY FROM RESONANCE
 - CONTINUUM DUE TO NON-RESONANT O₂ AND PRESSURE INDUCED ABSORPTION
 - HYDROSAL ATTENUATION MODEL (RAYLEIGH ABSORPTION FOR HAZE, FOG, AND CLOUDS)
 - PARAMETERIZED, POWER-LAW RAIN ATTENUATION MODEL TO SIMULATE M₀ SCATTERING

Figure 2.1.1 Comparisons of ARMSS-Predicted Atmospheric Attenuation With Published Data

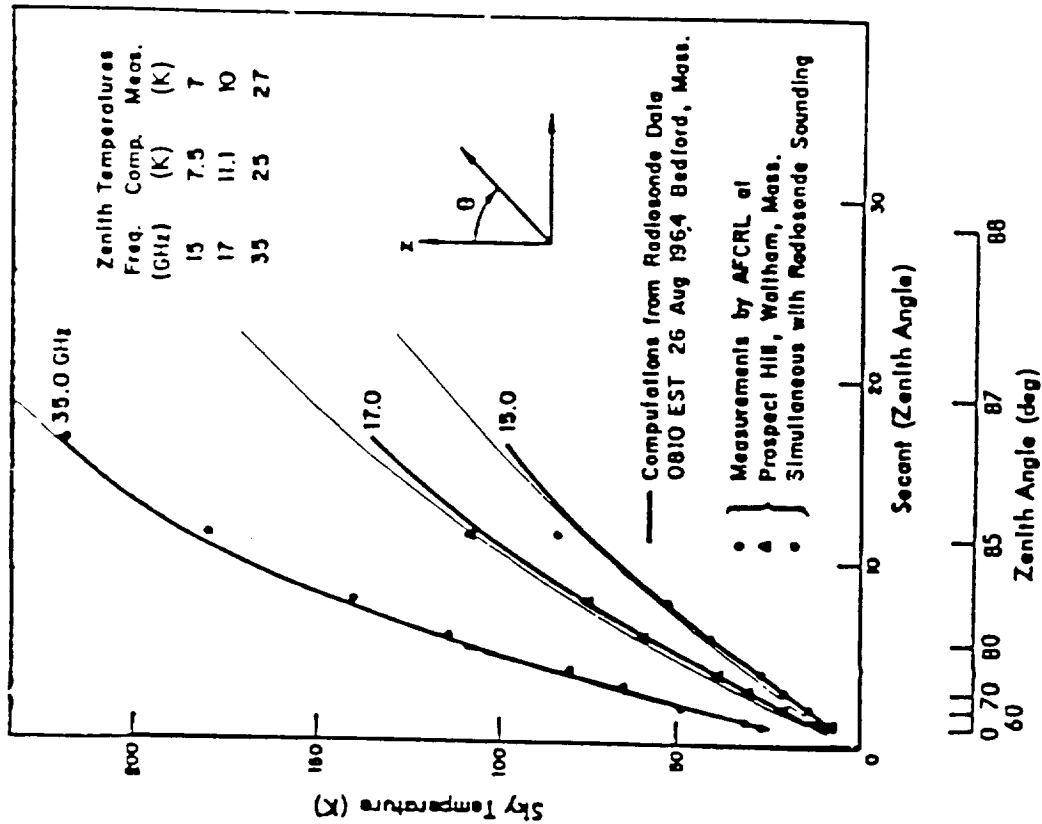
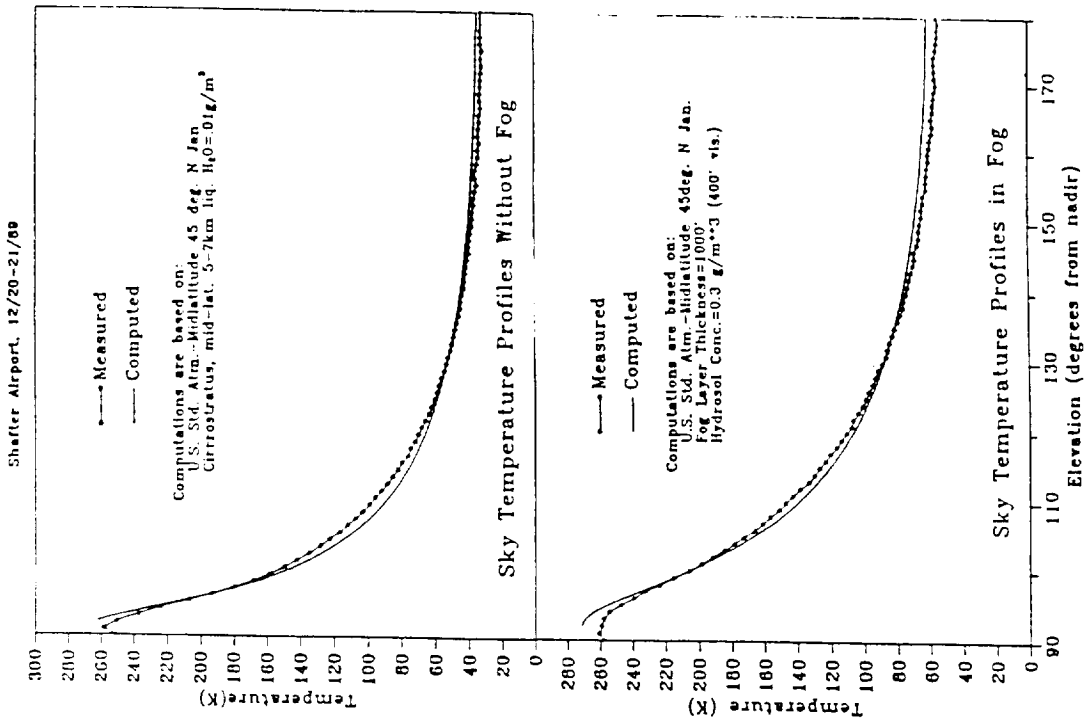


Figure 2.1.2 ARMSS-Predicted Sky Temperature Profiles Under Clear Air and Fog Conditions

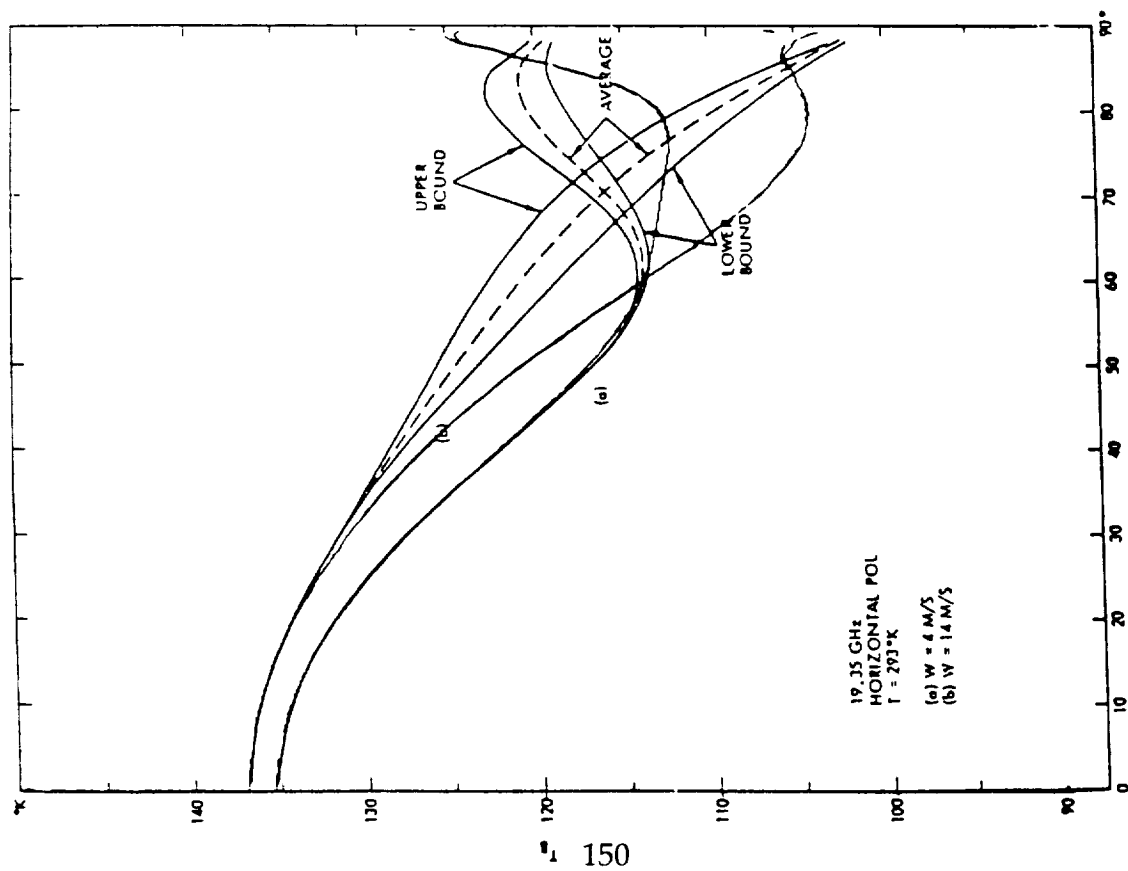
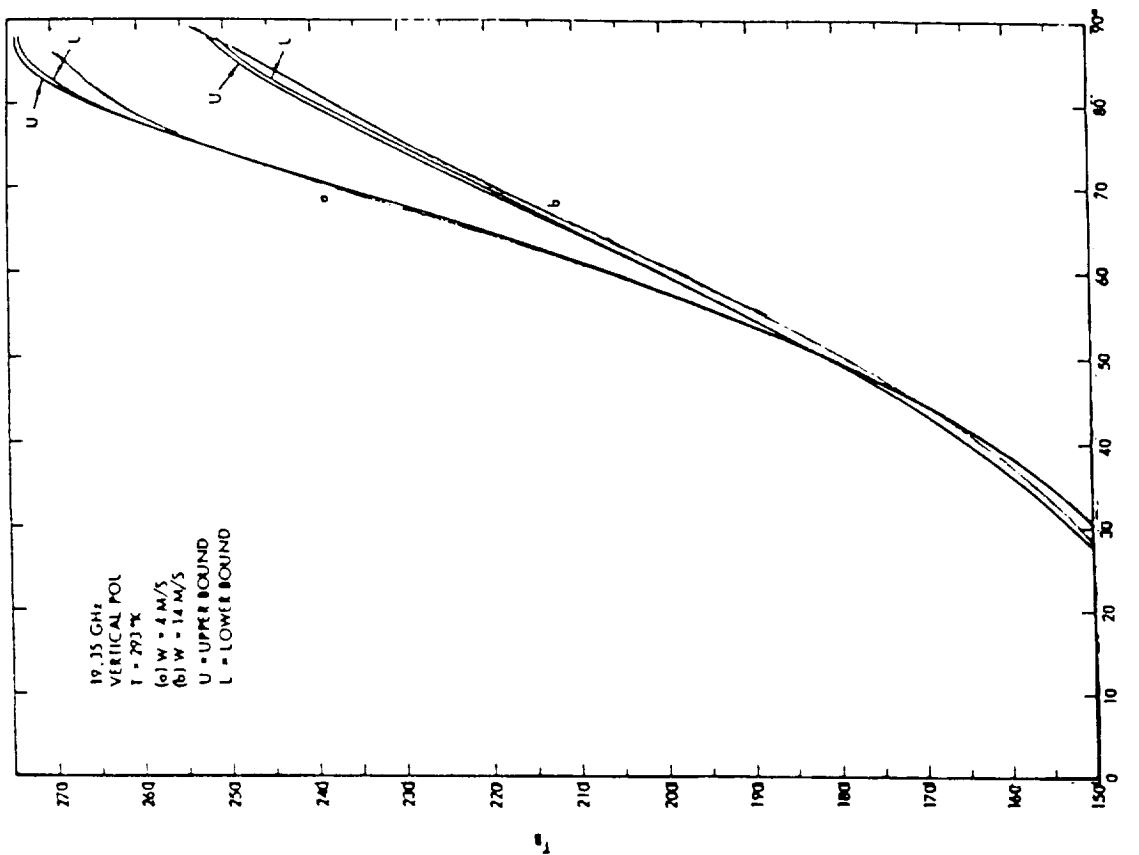


Figure 2.2.1 Comparison of ARMSS-Scatter and a Double-Scatter Surface Model for (a) Horizontal Polarization and (b) Vertical Polarization

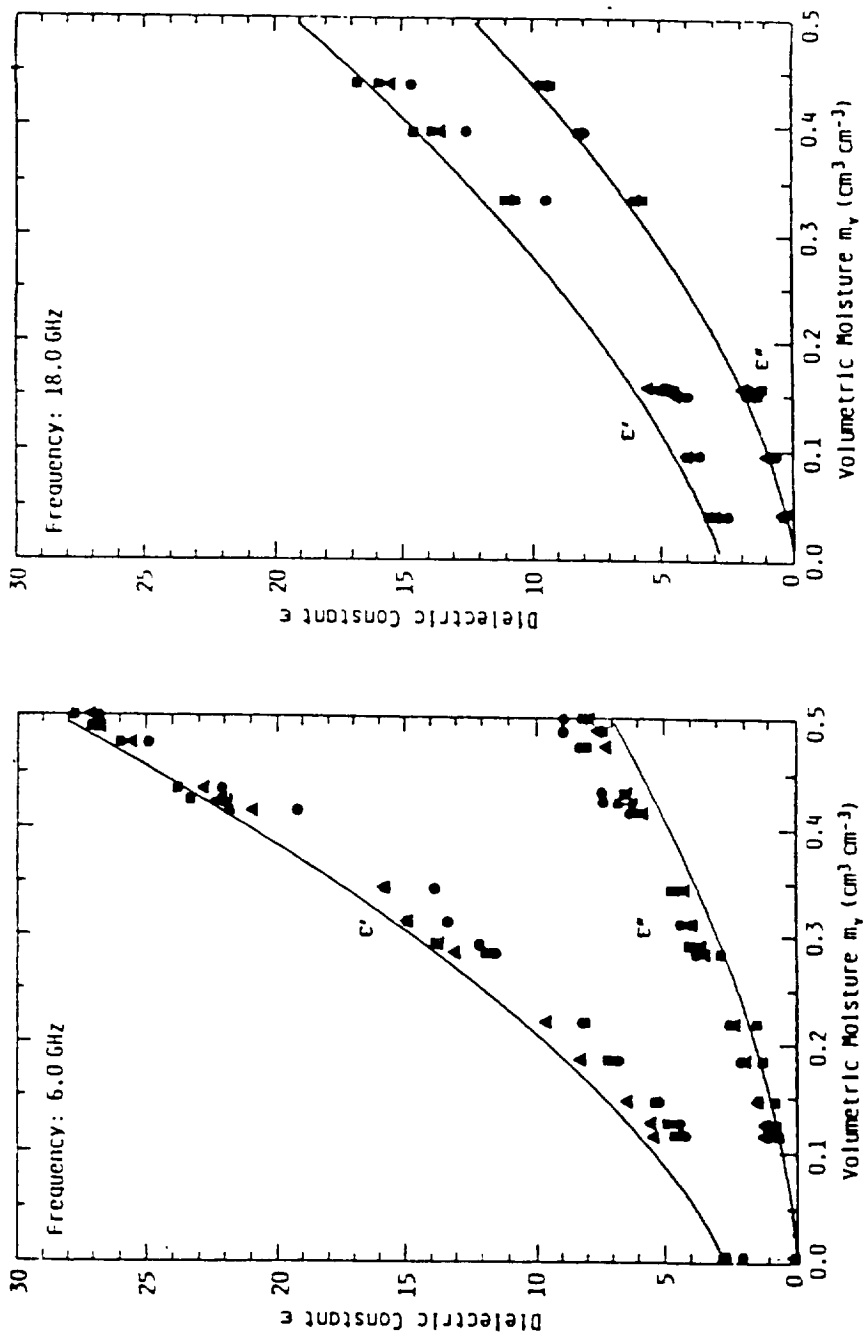


Figure 2.2.2 ARMSS-Predicted and Measured Dielectric Properties for a Silty Clay at (a) 6 GHz and (b) 18 GHz

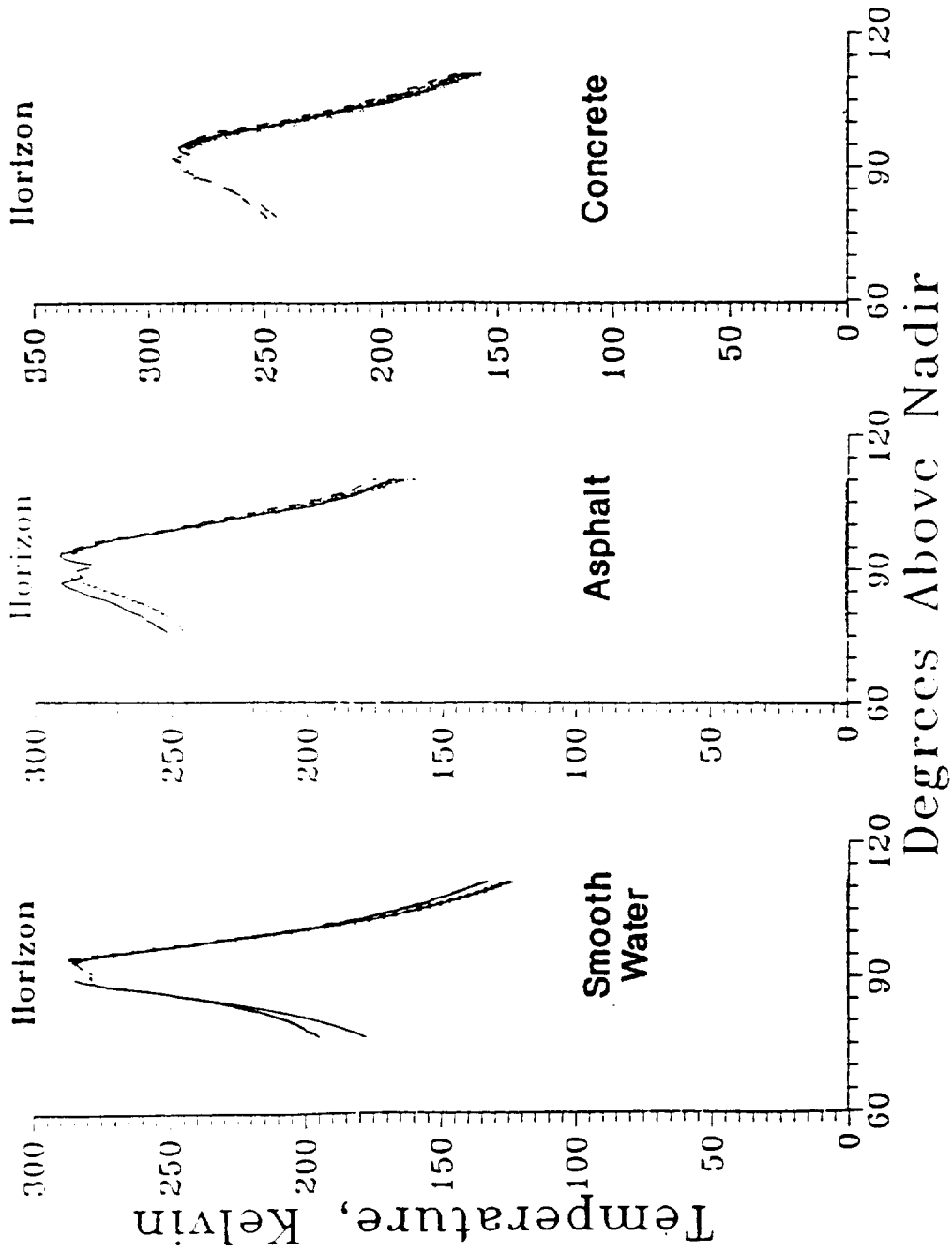


Figure 2.3.2 Measured and ARMSS-Predicted Radiometric Scans of Various Terrain Media

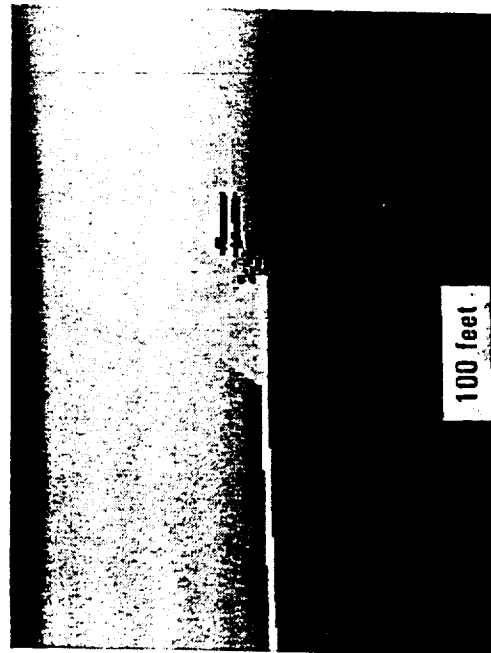
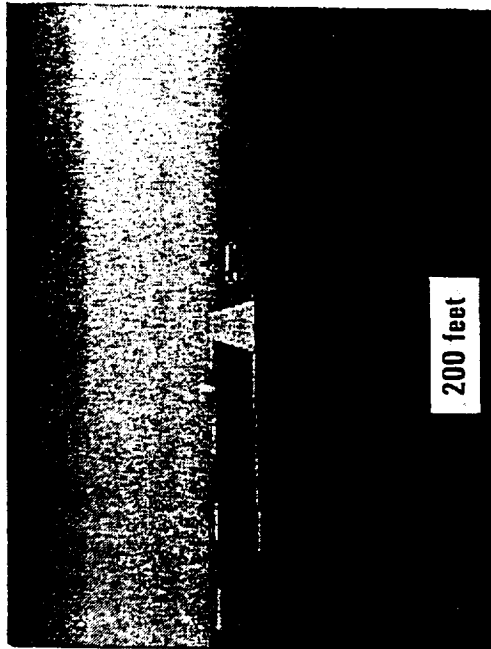
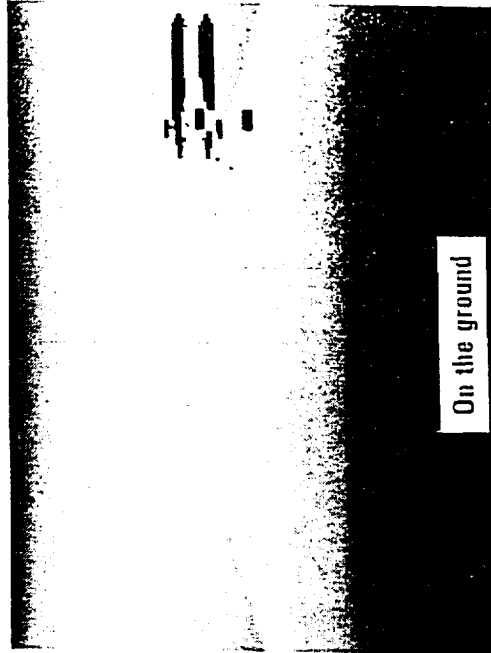
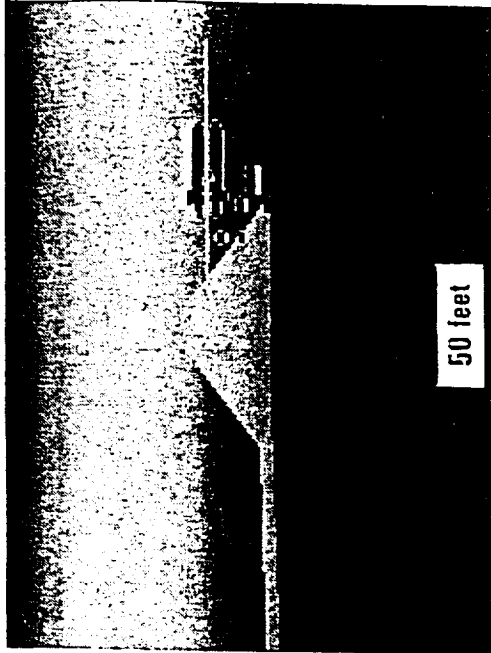


Figure 2.3.1.1 ARMSS-Generated High Resolution Millimeter Wave Runway Scenes Under Heavy Fog and Wet Surface Conditions

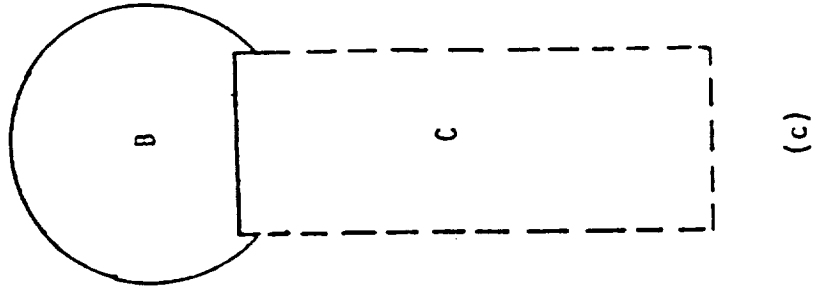
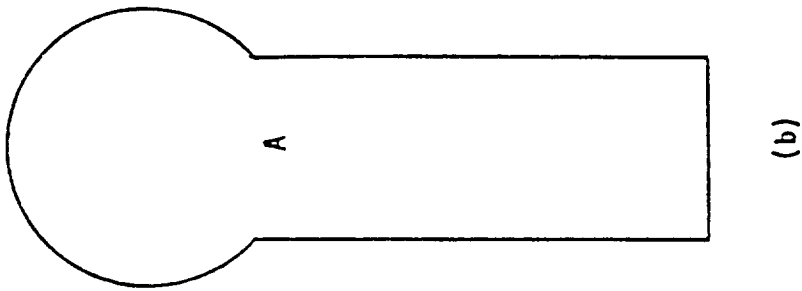
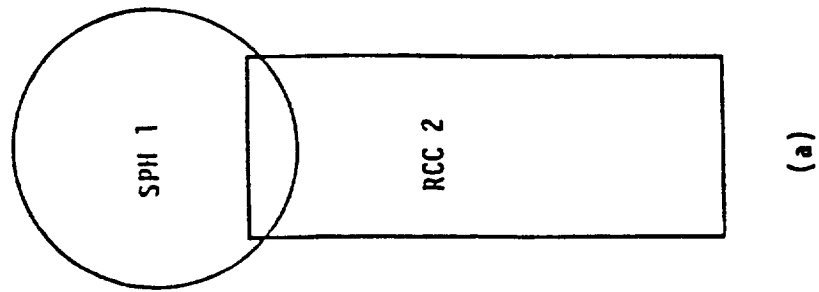


Figure 2.3.3 Three-Dimensional Objects Formed from (b) Union and (c) Exclusion of a Sphere and Cylinder

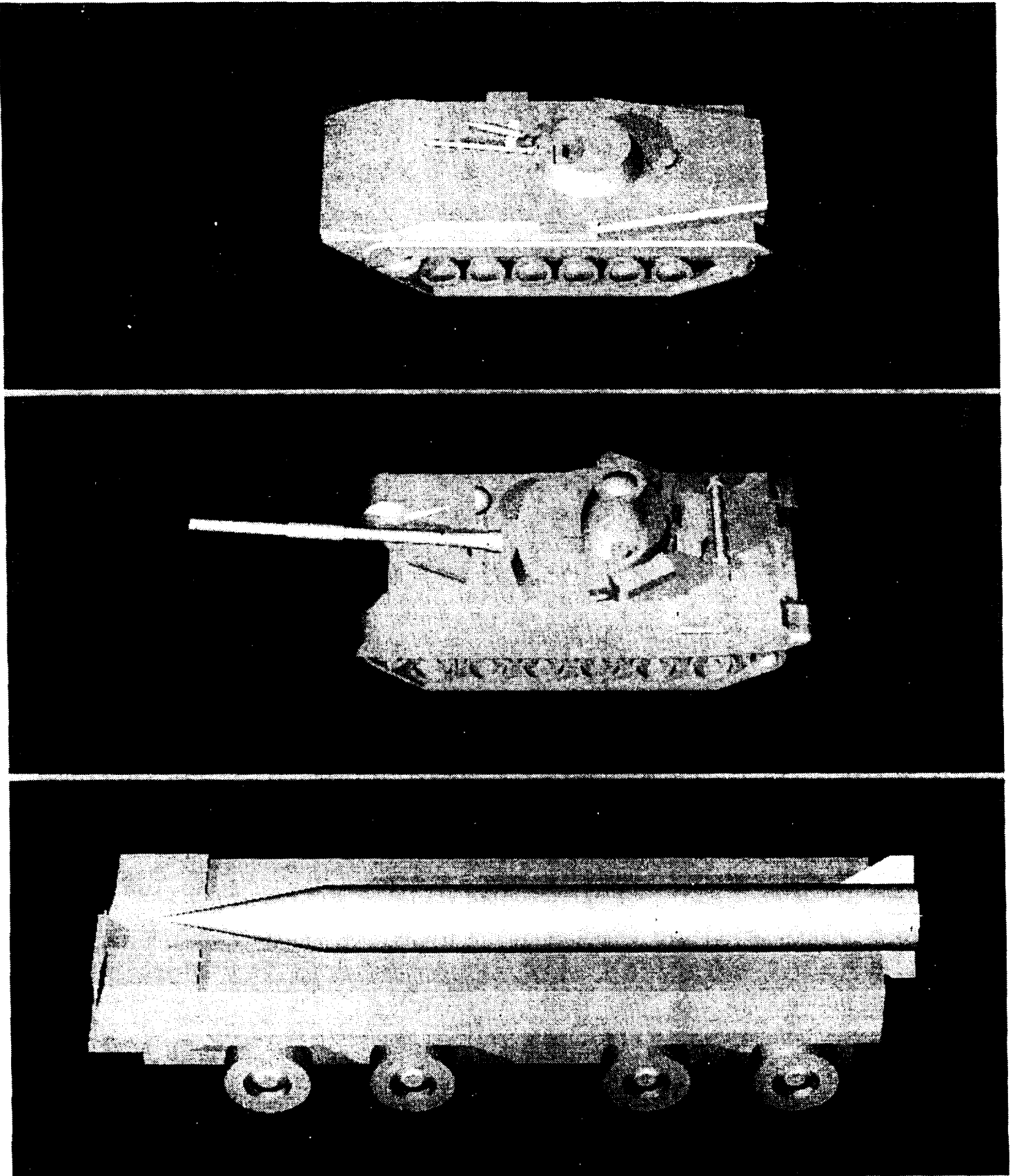


Figure 2.3.4 Combinatorial Geometry Models of BMP-1 Troop Transport, T-72 Tank, and SS-24 Missile and Mobile Launcher

Methods for Including Upwelling Atmospheric Radiation

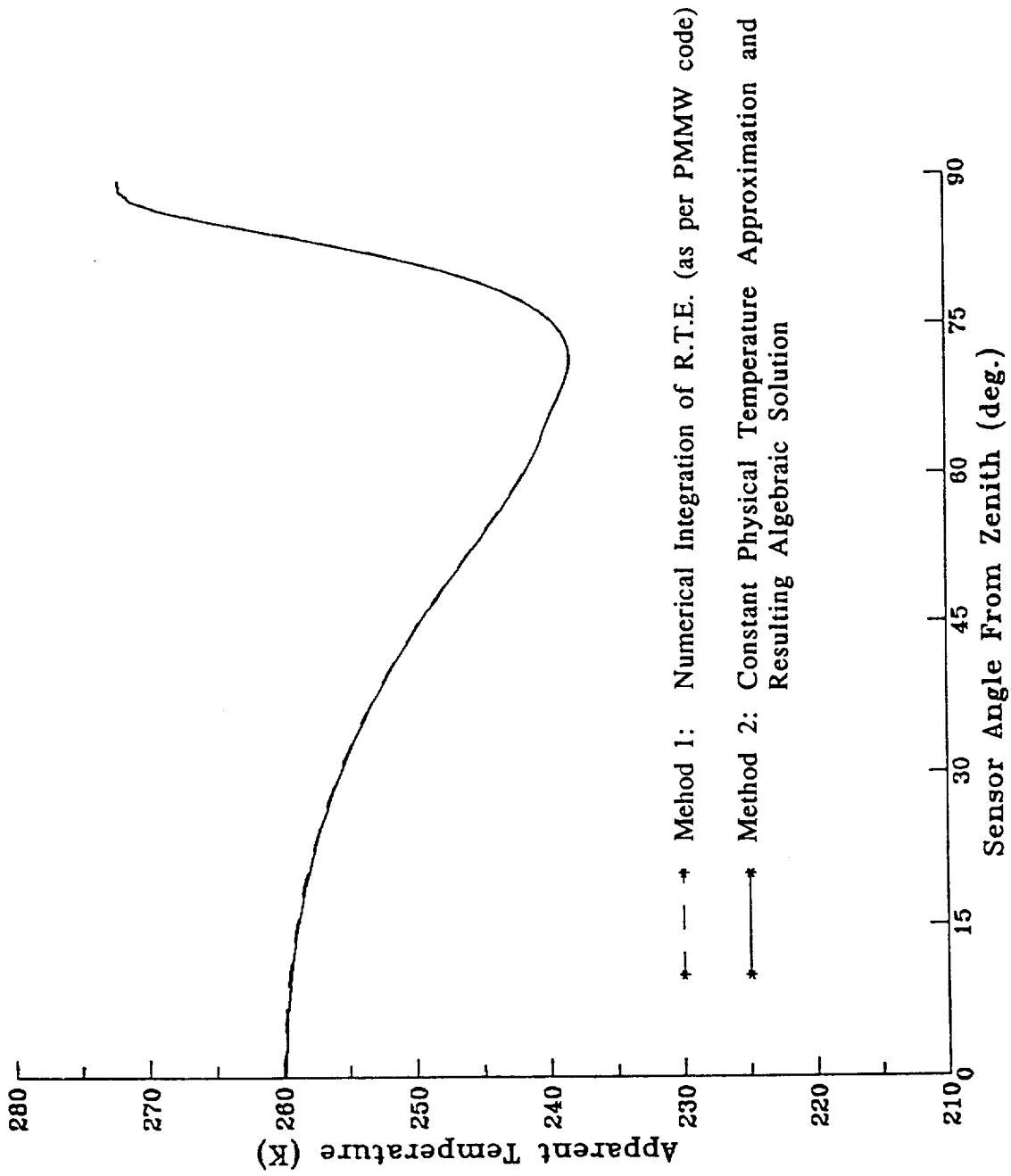
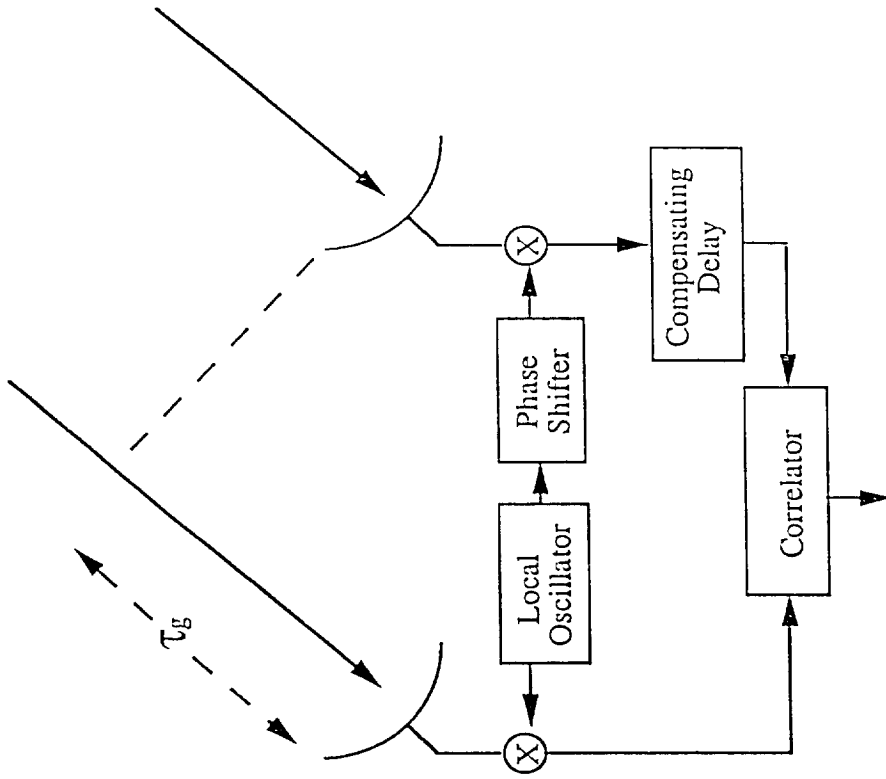


Figure 2.4.1

Figure 3.1

Two-element Interferometer Is The Building Block For The Interferometric Imager



- Correlator output "samples" a scene spatial frequency component
- Correlations between different apertures or at different frequencies produce additional "samples"
- Image is generated by Fourier Transform of "samples"
- Enhancement techniques applied to compensate for incomplete, or phase corrupted "samples"

$$V(u,v) = \iint A(l,m) I(l,m) e^{-2\pi i(ul+vm)} dl dm$$

Figure 3.2.1 LOW DENSITY AIRPORT SCENE

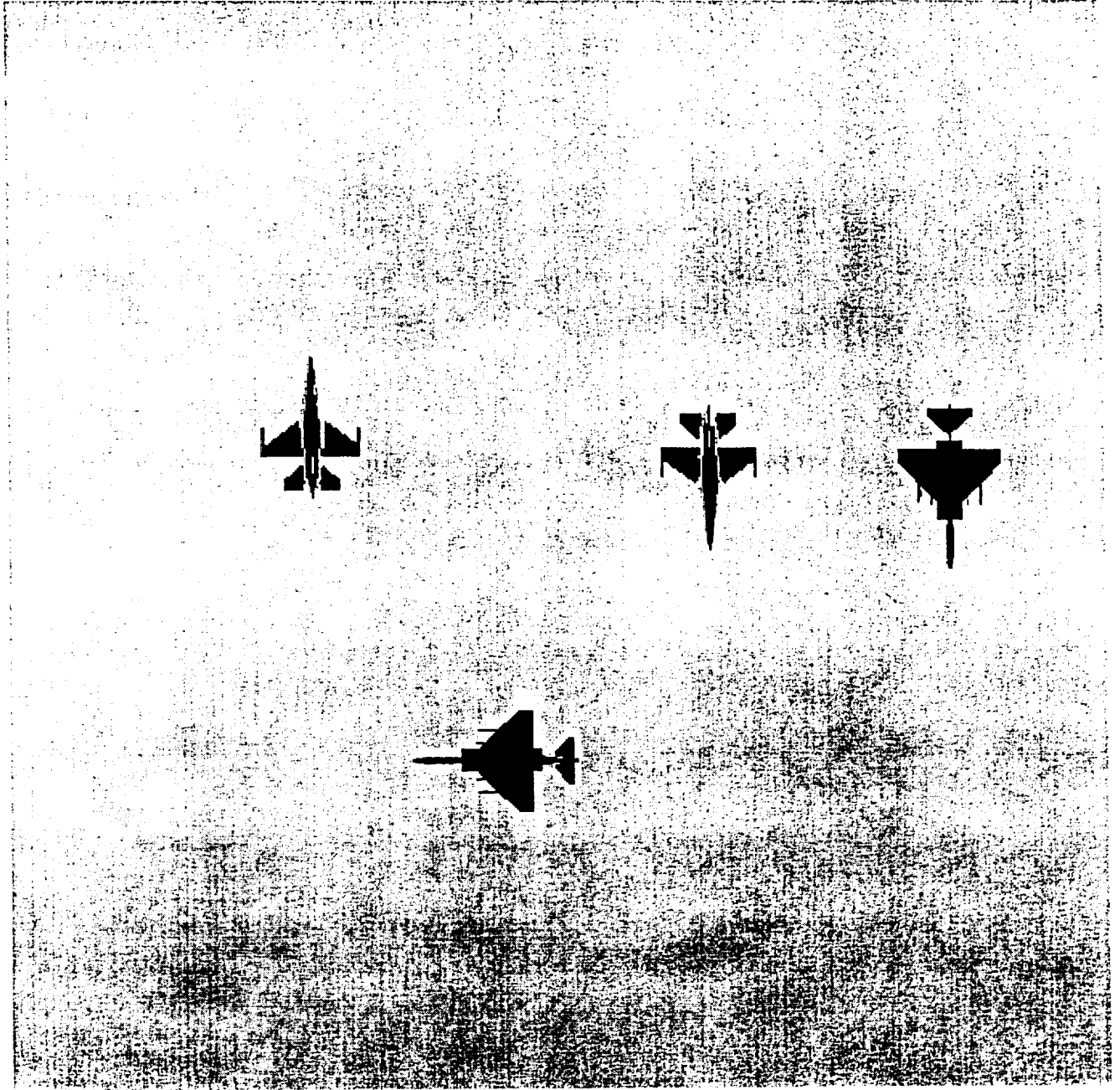


Figure 3.2.2

INTERFEROMETRIC SAMPLING

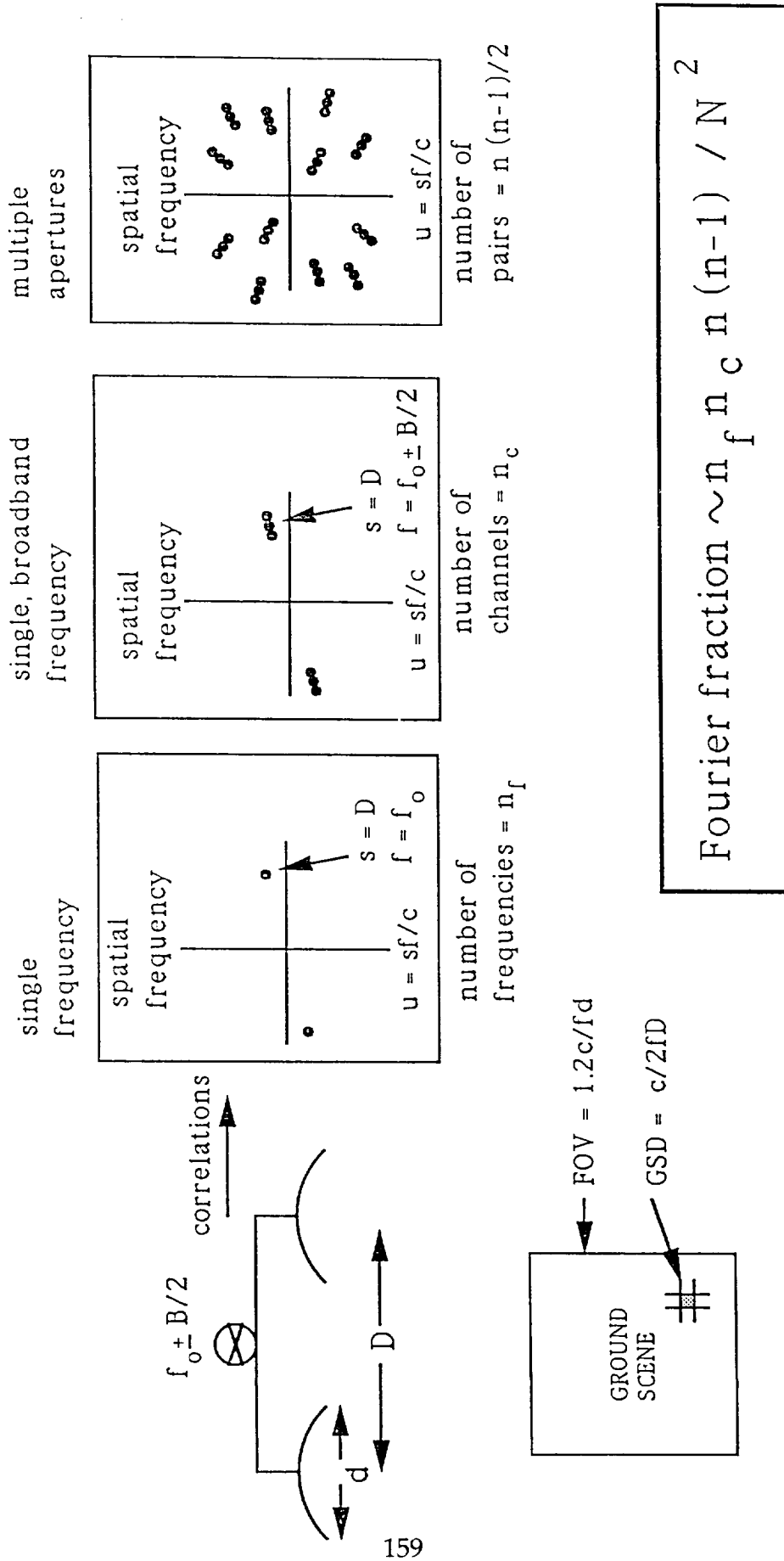


Figure 3.2.3

Procedure

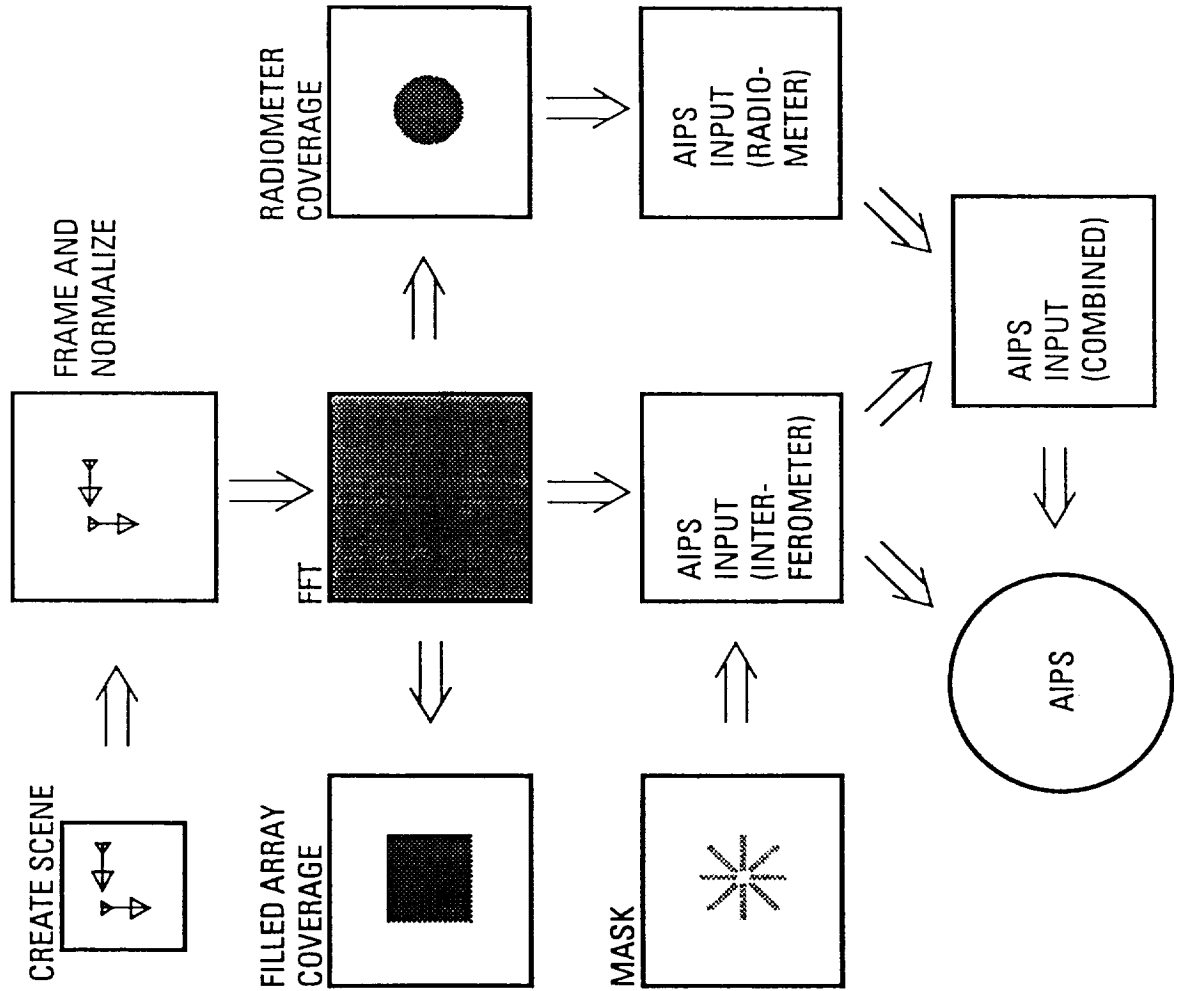
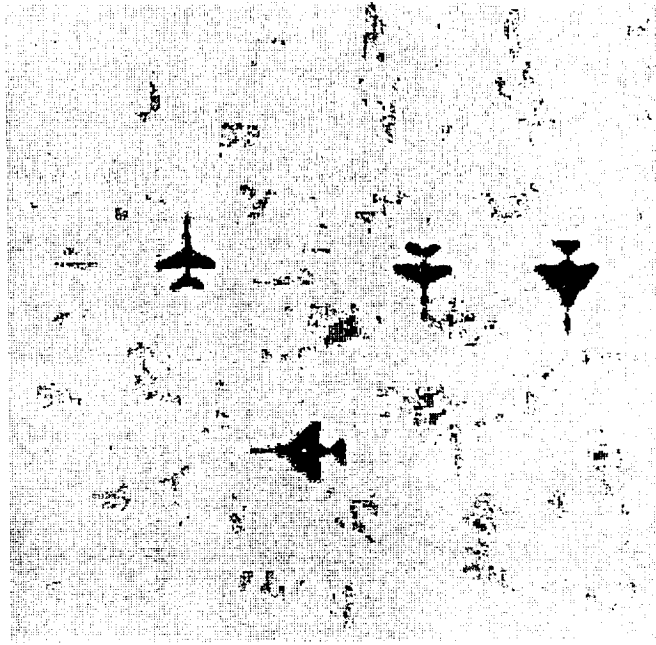
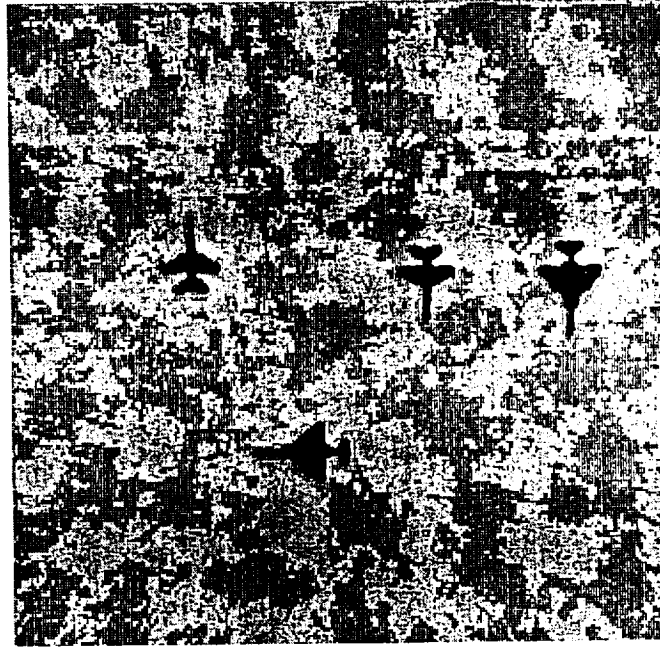


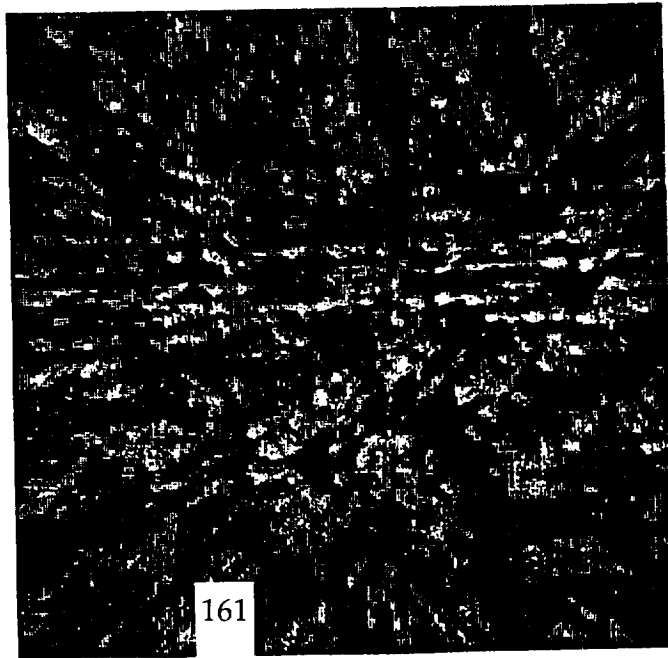
Figure 3.2.4 Unprocessed and Processed Images



MEM



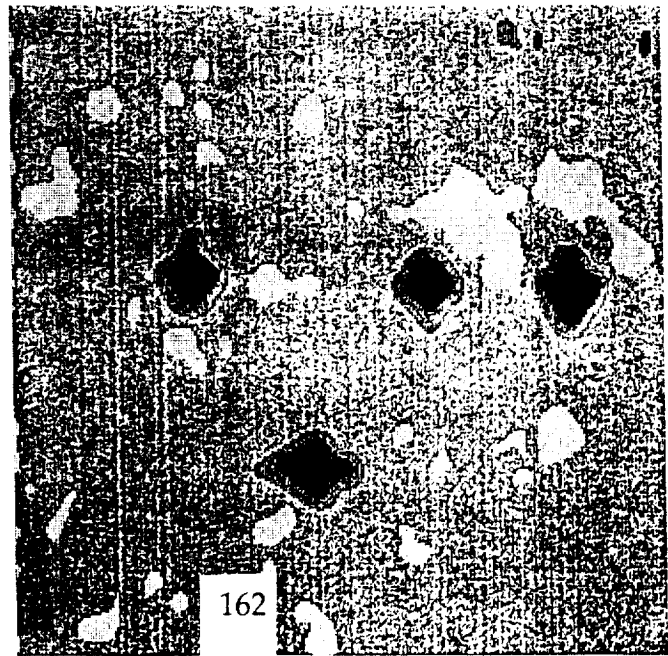
CLEAN



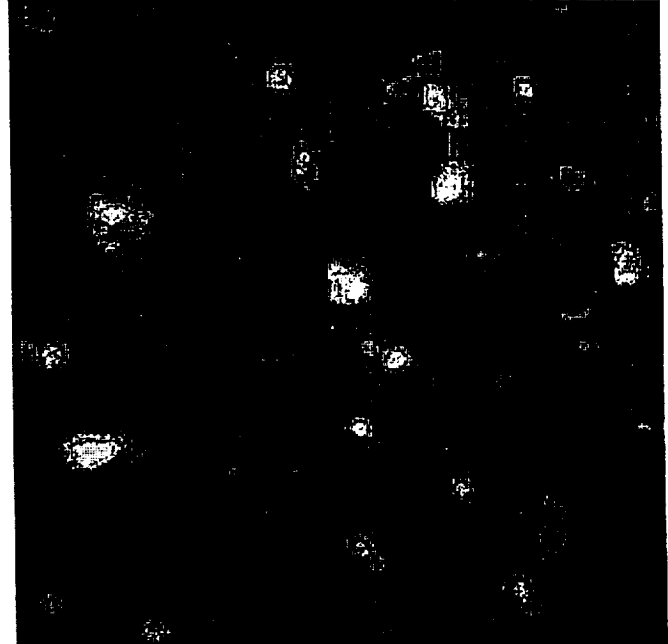
IMAGE

Figure 3.2.5

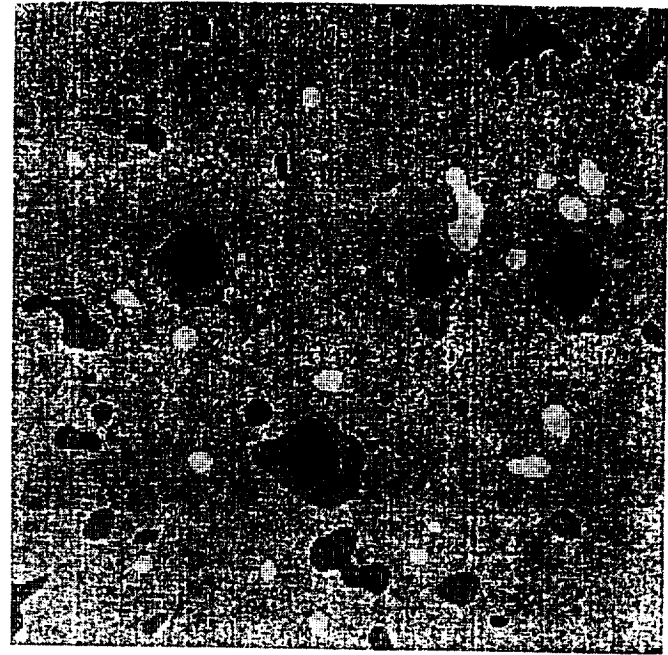
SELF-CALIBRATION CLEANED IMAGES



UNCORRUPTED



CORRUPTED



CALIBRATED